Supporting Information For:

Surface Interrogation Scanning Electrochemical Microscopy of $Ni_{1-x}Fe_xOOH$ ($0 < x < 0.27$) Oxygen Evolving Catalyst: Kinetics of the "fast" Iron Sites

Hyun S. Ahn and Allen J. Bard*

Contribution from the Center for Electrochemistry, Department of Chemistry, The University of Texas at Austin, Austin, Texas 78712, United States

Email: ajbard@mail.utexas.edu

Table of Contents	**Page**

[Fe(TEA)(OH)]$^-$ mediator synthesis. [Fe(TEA)(OH)]$^-$ mediator (TEA = triethanolamine $C_6H_{15}NO_3$) was synthesized by literature published method.[1,2] Briefly, 20 mL deionized water was deaerated, into which 0.40 mmol of ferric sulfate nonahydrate was added. To this solution 0.45 mmol of TEA was added with continued stirring. A separate solution of KOH (0.1 mol in 10 mL deionized water) was prepared and ice cooled. The KOH solution was then added dropwise to the stirring mixture of Fe^{3+} and TEA. The solution was allowed to keep stirring and slowly warmed up to room temperature for 1 h. The volume of the solution was adjusted by addition of deionized water to 50 mL. Each redox mediator solution prepared was used no more than 48 h. A cyclic voltammogram of the FeTEA mediator is shown below (E° = -1.05 V vs. Ag/AgCl, Scan rate = 50 mV/s).

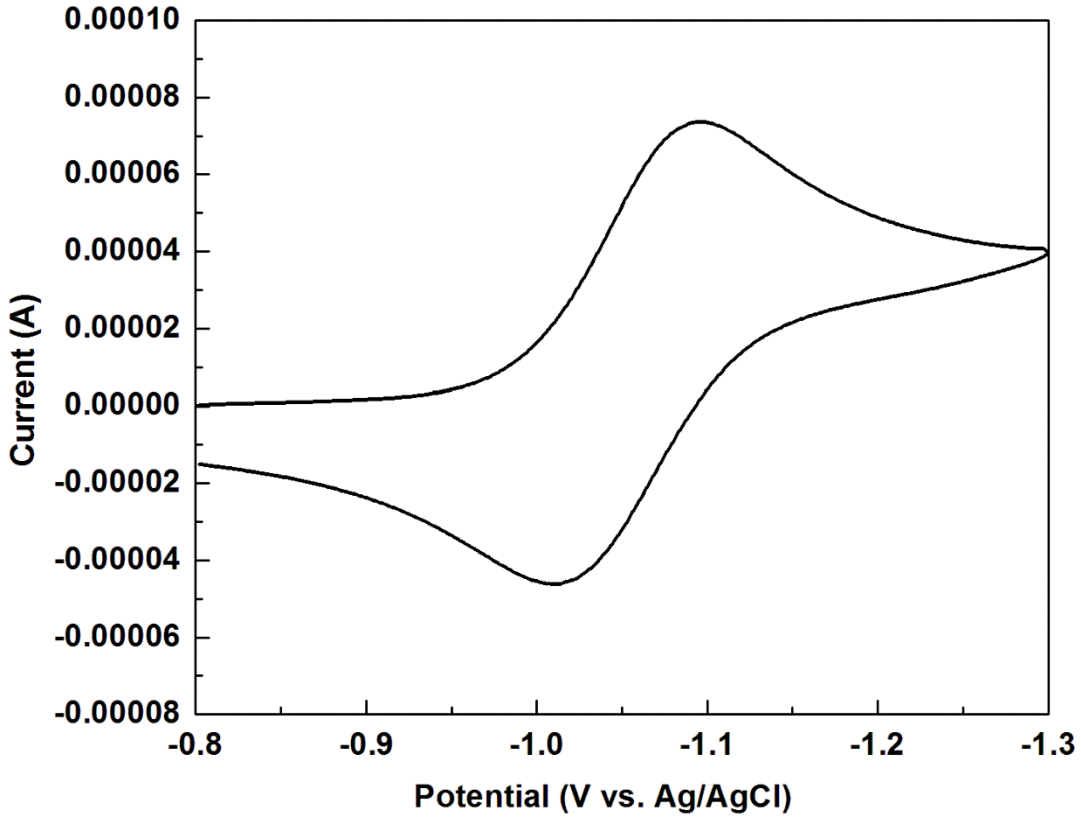

Figure S1. A cyclic voltammogram of [Fe(TEA)(OH)]$^-$ (glassy carbon electrode, diameter 2 mm, 8 mM FeTEA in 2 M KOH, 50 mV/s).

SI-SECM tip-substrate alignment and approach

The tip and substrate electrodes, both gold ultramicroelectrodes (UMEs) of radius a = 12.5 µm, were initially positioned at a close distance in a SECM cell by visually aligning the two. In a typical SECM cell, the tip and the substrate electrodes are positioned vertically (substrate UME pointing up and tip UME pointing down). Throughout the experiment the substrate electrode remains stationary (tilt corrected by a three-point stage positioner)[3] and the tip electrode's motion is controlled by inchworm stepper motors and piezo controllers in all three dimensions.[3] The tip and substrate UMEs serve as working electrodes to the bipotentiostat. Once the two electrodes were positioned, the cell was filled with the analyte solution (8 mM $[Fe(TEA)(OH)]^-$ in 2 M KOH). A potential bias was applied on the substrate electrode to induce positive feedback (600 mV) as the tip was scanned across it. A current profile (2D slice, X or Y at a constant Z position) of the contour of the substrate UME and the surrounding glass sheath was obtained as shown in Figure S2. Tip-substrate alignment was carried out by scanning the tip over the substrate in X and Y and positioning the tip at the position where maximum positive feedback occurred. The tilt of the stage was corrected by obtaining a current profile shown in Figure S2 and repeating the scan as the tilt of the stage was varied both in X and Y until a current profile symmetrical with respect to the vertex was obtained. Once the tilt correction and tip-substrate alignment were achieved, the tip was then slowly approached to the substrate in the Z direction (rate 50 nm per second) yielding a positive feedback approach curve in good agreement with theory displayed in Figure S2. The tip electrode was positioned at 2 µm away from the substrate (calculated from positive feedback current) before SI-SECM experiments began.

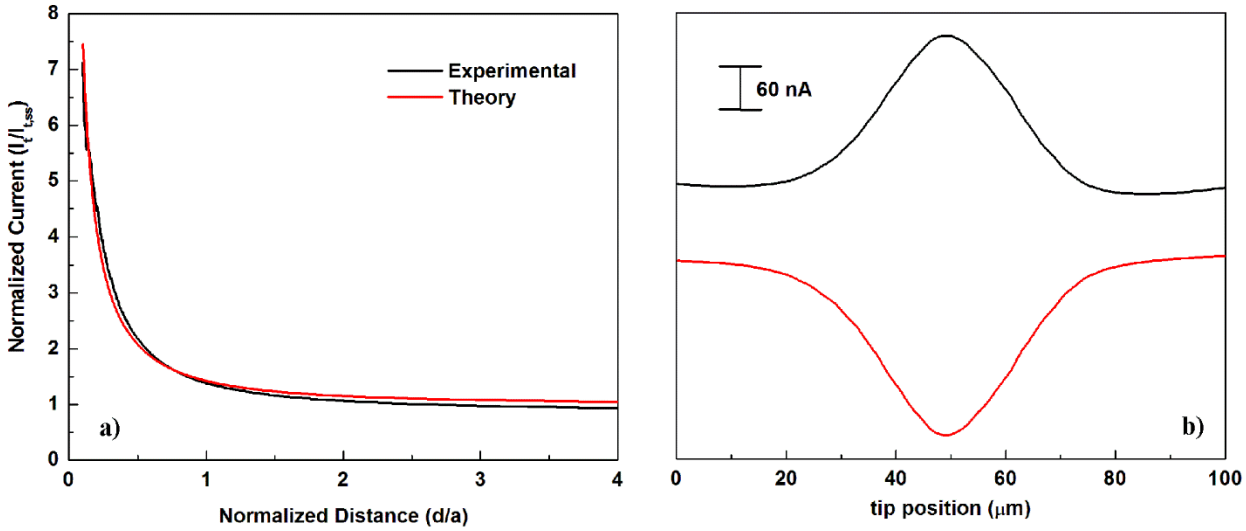

Figure S2. A positive feedback approach curve (left) of the tip UME on a substrate UME. For details on theory, see reference 3. A scan in the X of the tip over the substrate at a Z distance of *ca.* 5 µm (right; tip-current in black and substrate-current in red). The alignment and tilt-correction process was repeated in the X and Y to obtain good approach for surface interrogation.

Measurement of the pseudo first-order OER rate constants

As discussed in the manuscript, in our experimental setup, a pseudo-first order rate constant of Ni^{IV} can be measured by varying the parameter t_{delay}. Because the titrant (FeTEA) is formed at the tip only after t_{delay}, during t_{delay} the only reagent reacting with the surface active species is water. A simplest example case is shown below.

$$Ni^{IV} + H_2O \rightarrow Ni^{III} + OH\cdot_{(ads)} + H^+$$

Pseudo First-Order Rate Equation

$$\frac{dNi^{IV}}{dt} = -k'[Ni^{IV}]$$

$$\ln[Ni^{IV}] = -k't + \ln[Ni^{IV}]_0$$

$$[Ni^{IV}] \quad [=] \quad mol \cdot m^{-2}$$

From the relationship above, a pseudo-first order rate constant k' may be obtained by plotting ln $[Ni^{IV}]$ as a function of t_{delay} (see Figure S3 and Figure 1c). Similar analyses were applied to FeOOH and $Ni_{1-x}Fe_xOOH$ electrodes.

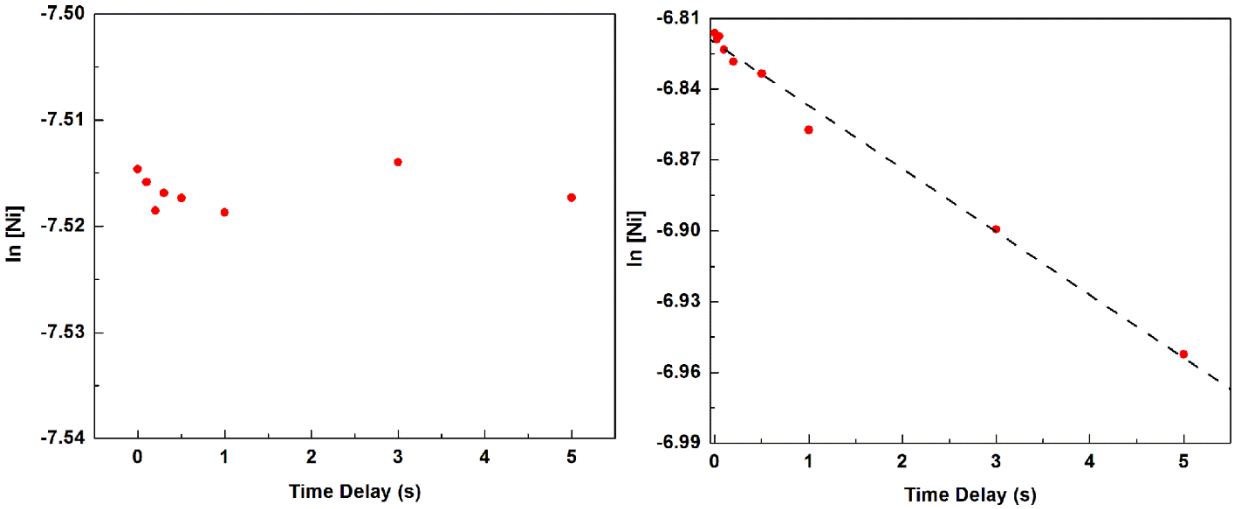

Figure S3. A time-dependent titration performed on a NiOOH (Ni^{III}) at E_{subs} = 0.5 V (left). No apparent decay in the titration feedback current occurred as a function of t_{delay}, indicating that Ni^{III} in NiOOH is inactive for OER in the several seconds time. In the right frame, a supplement figure to that shown in Figure 1c is displayed (time-dependent titration of Ni^{IV} at E_{subs} = 0.6 V, with time data up to 5 s).

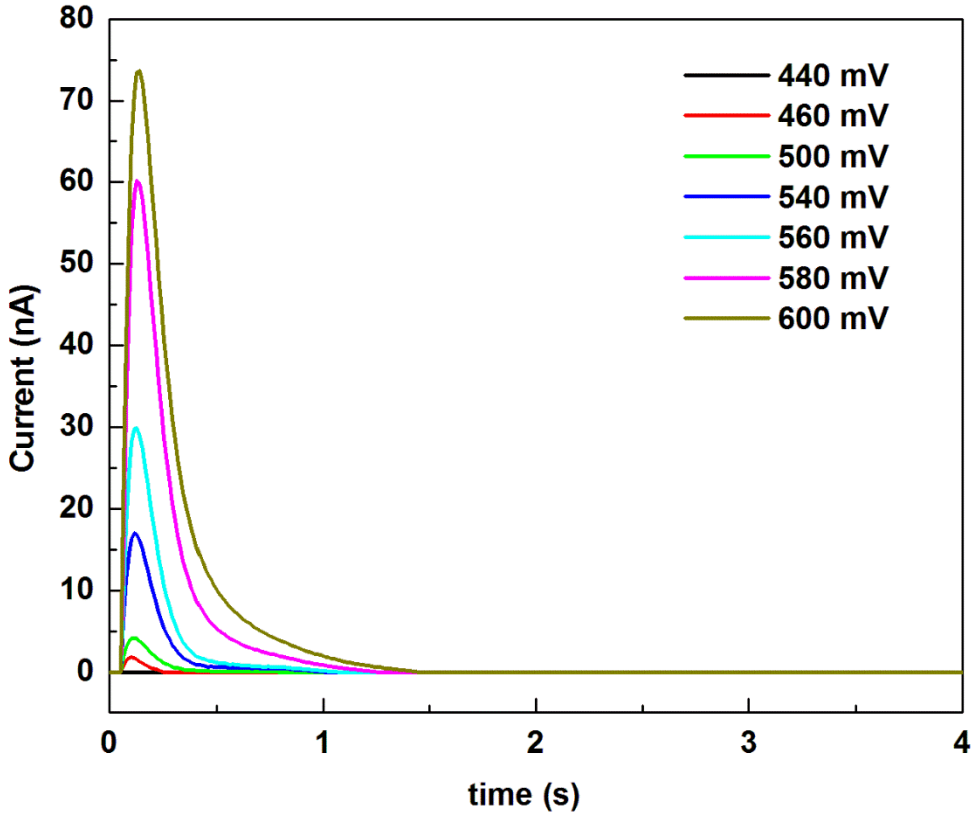

Figure S4. Titration CA traces obtained from surface titrations of FeOOH at varying E_{subs} (shown in inset label). The integrated charge under the curves were projected as a redox titration curve shown in Figure 1b.

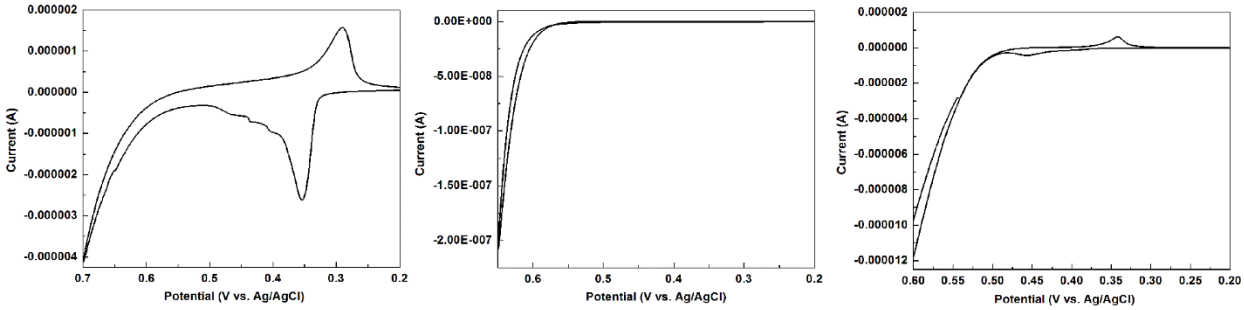

Figure S5. Cyclic voltammograms (CVs) of $Ni(OH)_2$ (left), FeOOH (center), and $Ni_{0.82}Fe_{0.18}OOH$ (right), respectively in 2 M KOH. No redox feature was observed in FeOOH in the potential range of interest (0.2 – 0.7 V) aside from OER occurring at 0.6 V, suggesting that all irons in the FeOOH film are in Fe^{III} state – consistent with the findings from XAS studies.[4] In the CV of $Ni(OH)_2$, a shoulder in following the $Ni^{III/II}$ oxidation peak at *ca.* 0.45 V was observed. This shoulder is a common feature when the $Ni(OH)_2$ is pure and free of iron contaminants.[5] The CV of $Ni_{0.82}Fe_{0.18}OOH$ is similar to those reported in the literature for 10 – 20 % iron doped nickel.[5]

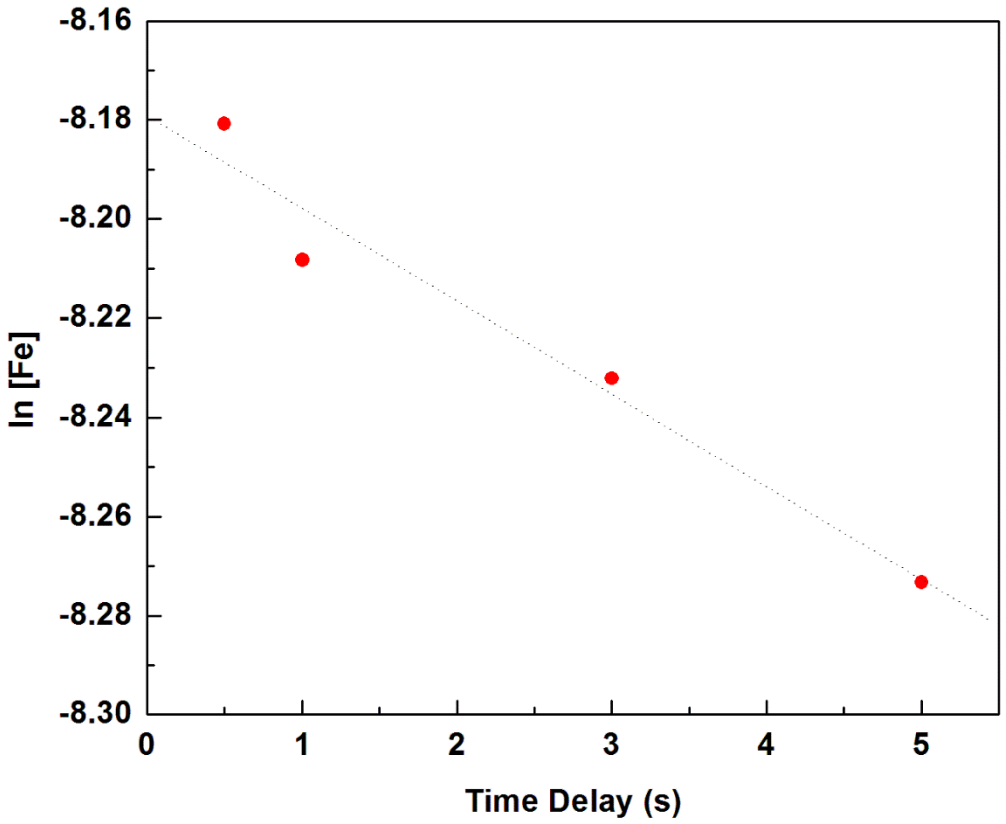

Figure S6. Time-dependent titration of FeOOH at extended delay times (0.5 – 5.0 s). This figure should supplement those shown in Figure 2.

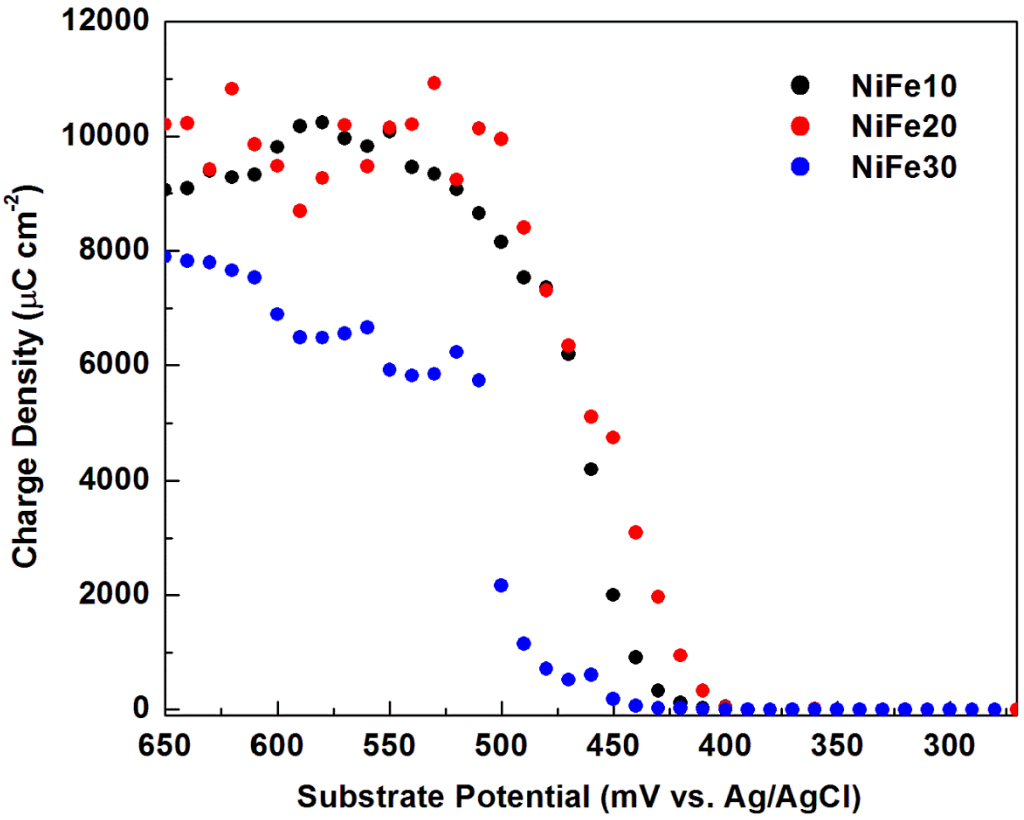

Figure S7. Redox titration curves for $Ni_{0.91}Fe_{0.09}OOH$ (NiFe10), $Ni_{0.82}Fe_{0.18}OOH$ (NiFe20), and $Ni_{0.73}Fe_{0.27}OOH$ (NiFe30) electrodes. Significant phase segregation (titration curve similar to that of $Ni(OH)_2$; Figure 1b) shown in $Ni_{0.73}Fe_{0.27}OOH$ electrode.

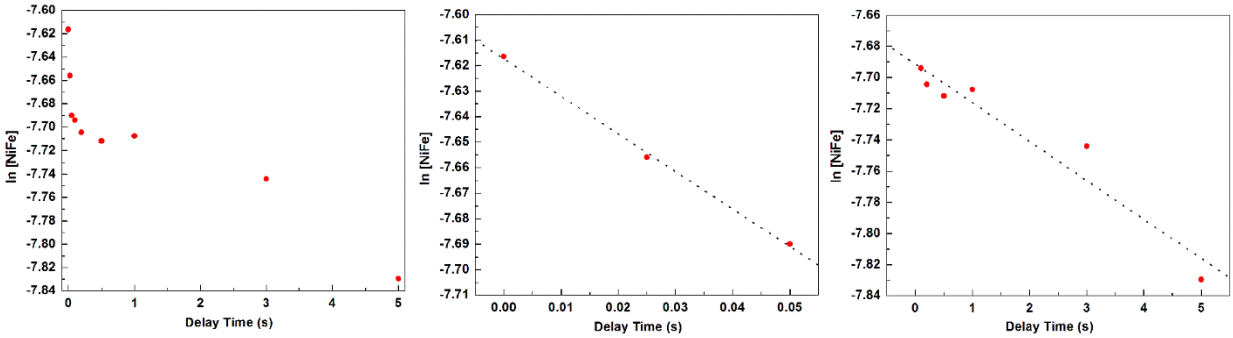

Figure S8. Time-dependent titration behavior of the $Ni_{0.82}Fe_{0.18}OOH$ electrode at E_{subs} = 0.45 V (left). A time dependent decay in the titration current was observed, indicating OER. The OER catalysis occurred at a much more cathodic (> 0.15 V positive) potential than those observed from NiOOH and FeOOH. Two linear regions were best fit when the times were selected as presented above: "Fast" sites up to 50 ms (center) and the rest in "Slow" site time scale (right). The OER rate constants obtained from the "Fast" site fit was 1.47 ± 0.11 s^{-1}, and that of the "Slow" sites was 0.03 ± 0.02 s^{-1}. The "Fast" site fraction at this E_{subs} (0.45 V) was 7.1 %, significantly less than the iron content in the film (18.19 %) and that observed at a higher E_{subs} (0.6 V, 17.6 %). This presumably arises from the non-homogeneous surface energy distribution in the solid, and the high barrier to reach the active Fe^{IV}. A similar behavior was seen for Co^{IV} in a cobalt oxide catalyst in our previous investigation.[6]

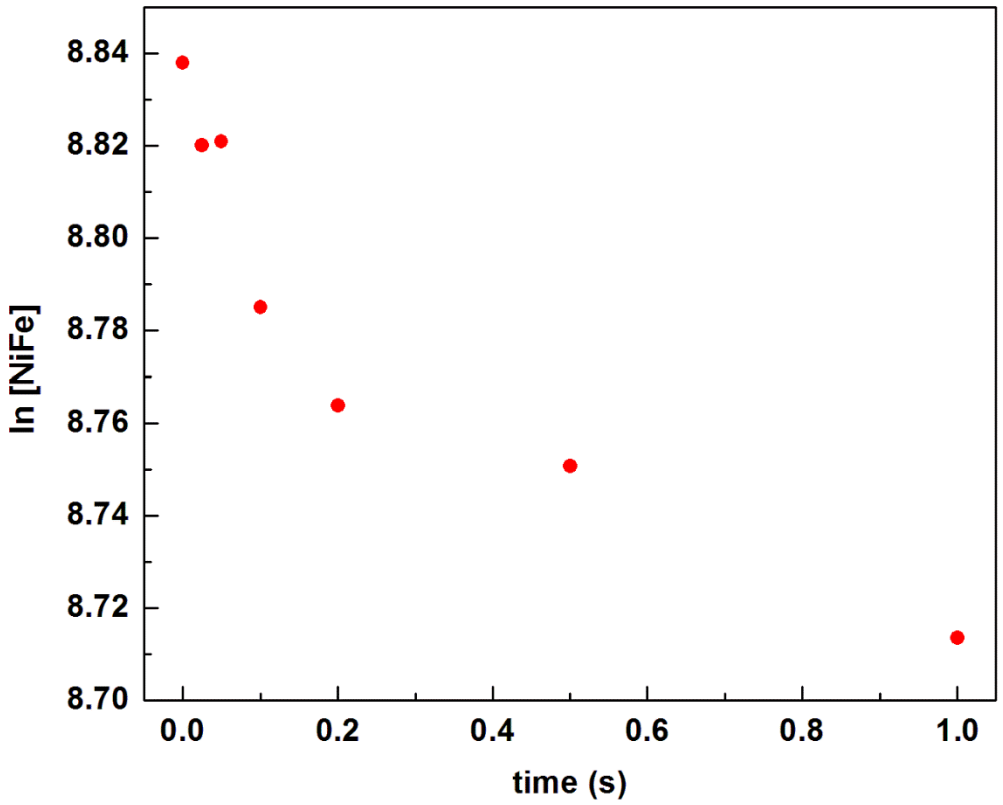

Figure S9. The time-dependent titration behavior of the $Ni_{0.73}Fe_{0.27}OOH$ electrode at E_{subs} = 0.6 V. No clear discrimination in the two linear zones corresponding to "Fast" and "Slow" sites were observed. As seen in the titration curve (Figure S7), probably a phase segregation into NiOOH and FeOOH had occurred.

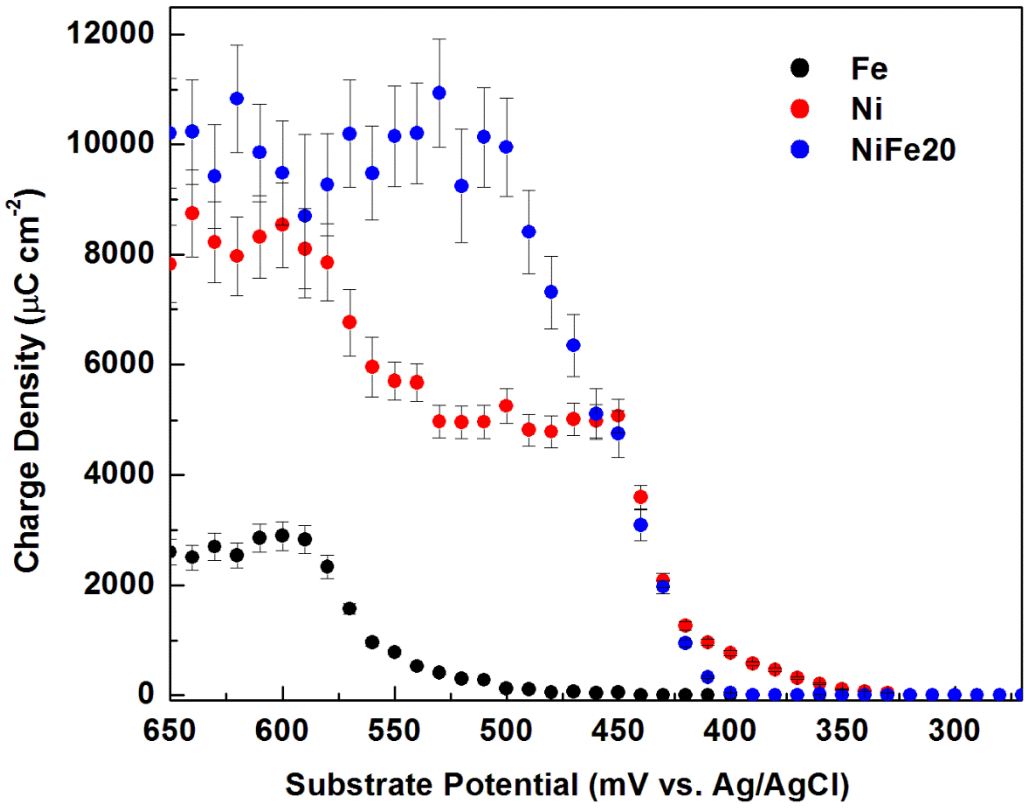

Figure S10. Redox titration curves of $Ni(OH)_2$, FeOOH, and $Ni_{0.82}Fe_{0.18}OOH$ with error bars. On average, the errors were smaller than 6 % at $E_{subs} < 0.5$ V, and 9 – 10 % at $E_{subs} > 0.5$ V.

References

1. Bechtold, T.; Burtscher, E.; Gmeiner, D.; Bobleter, O. *J. Electroanal. Chem.* **1991**, *306*, 169.
2. Arroyo-Curras, N.; Bard, A. J. *J. Phys. Chem. C* **2015**, *119*, 8147.
3. Bard, A. J.; Mirkin, M. V. *Scanning Electrochemical Microscopy, Second Edition*; 2 edition.; CRC Press: Boca Raton, 2012.
4. Friebel, D.; Louie, M. W.; Bajdich, M.; Sanwald, K. E.; Cai, Y.; Wise, A. M.; Cheng, M.-J.; Sokaras, D.; Weng, T.-C.; Alonso-Mori, R.; Davis, R. C.; Bargar, J. R.; Nørskov, J. K.; Nilsson, A.; Bell, A. T. *J. Am. Chem. Soc.* **2015**, *137*, 1305.
5. Trotochaud, L.; Ranney, J. K.; Williams, K. N.; Boettcher, S. W. *J. Am. Chem. Soc.* **2012**, *134*, 17253.
6. Ahn, H. S.; Bard, A. J. *J. Am. Chem. Soc.* **2015**, *137*, 612.